Shock Compression of Organic Polymers and Proteins: Ultrafast Structural Relaxation Dynamics and Energy Landscapes

Hackjin Kim,[†] Selezion A. Hambir, and Dana D. Dlott*

School of Chemical Sciences, University of Illinois at Urbana-Champaign, Box 01−6 CLSL, 600 S. Goodwin Ave., Urbana, Illinois 61801

Received: November 23, 1999; In Final Form: February 11, 2000

The response of organic polymers and proteins including poly(methyl methacrylate) (PMMA) and the protein bovine serum albumin (BSA) to a short duration 4.5 GPa shock pulse, termed a "nanoshock", is studied using ultrafast coherent Raman spectroscopy (CARS) to monitor density-dependent vibrational frequency shifts of a dye molecule probe. In conventional shock compression experiments, a two-part response of PMMA to fast compression is usually explained with a phenomenological viscoelastic model. The molecular basis for this two-part response is discussed here using an energy landscape model to describe large-amplitude structural relaxation of shocked supercooled liquids. The polymers and the protein show an instantaneous response to the steeply rising shock front, viewed as a vertical transition to a new region of the energy landscape with radically different topography. A slower ∼300 ps response is also observed, attributed to large-amplitude structural relaxation along the rugged shocked energy landscape. A viscoelastic model is used to determine an effective shock viscosity $\eta \approx 3$ Pa·s for the solid samples. This extremely small value (compared to $\eta > 10^{12}$ Pa·s expected for supercooled liquids) is explained as a result of the very large strain rate and the extensive plastic deformation, which causes even seemingly rigid solids to flow. After the short duration (∼2 ns) nanoshock unloads and the samples become frozen, for at least tens of nanoseconds, in a state where the dye vibrational shift indicates a negative pressure of about −1 GPa. The negative pressure means the local density near the dye has decreased, the sample has become more permeable, and the sample is unstable to spontaneous expansion of the polymer chains. The energy landscape model provides a framework for understanding the fast cycle of compression and expansion and how to optimize the generation and detection of large-amplitude structural relaxation processes.

1. Introduction

In this paper we use the nanoshock technique[1,2] to investigate ultrafast large amplitude structural deformation and structural relaxation of organic polymers and proteins. Shock compression experiments on polymers are usually discussed in the context of phenomenological viscoelastic models.[3−5] The molecular basis for this viscoelastic behavior is investigated with molecular spectroscopy during shock compression, and the results are interpreted in the context of a recently developed energy landscape model.[6]

Slowly occurring small-amplitude structural relaxation processes of supercooled liquids triggered by weak external mechanical, electrical, thermal, and optical perturbations have been discussed extensively.[7,8] These relaxation processes have been interpreted as resulting from transitions between local energy minima on a potential energy landscape.[9] Ordinarily, only the regions near the global minimum of the energy landscape are populated.[9]

Little is known about large-amplitude structural evolution in the higher energy regions of the potential energy landscape. Static high pressure can be used to produce large-amplitude strain. In 1929 it was shown that solidification of organic glass-forming liquids by cooling under high pressure produced glasses at ambient pressure which were somewhat denser than those formed by cooling at ambient pressure.[10] Price[11] showed that a stable "densified" state of poly(methyl methacrylate) (PMMA) could be produced, where the density increase was as large as 1.43%. Rapid heating and cooling of plastics (typically a few tens of K/s) during molding or extrusion can cause structural relaxation to fall behind the temperature, producing a stable state of small-amplitude (say <1%) strain, or a metastable state which undergoes slow volume recovery termed "creep".[8,12]

Fast, large-amplitude deformation of organic polymers has traditionally been investigated by shock compression science,[5] which has concentrated almost exclusively on PMMA,[5,13,14] although limited data on a few other polymers have appeared.[15,16] Here we investigate molecular-level processes involved in shock-compression-induced viscoelasticity using time-resolved spectroscopy of a molecular probe and a new energy landscape model. This work represents the first application of the energy landscape view to problems in shock compression. A brief report of the energy landscape work has been published.[6,17]

Conventional shock experiments typically involve high-speed projectile impact, producing step-function shock compression which can be probed by a fast strain-gauge or by velocity interferometry (VISAR).[15,18] A two-part "viscoelastic" response to the shock has been observed, as depicted in Figure 1a. The shock front is a steeply rising uniaxial stress wave. The first part of viscoelastic compression is an instantaneous elastic

* To whom correspondence should be addressed. Phone: 217-333-3574. Fax: 217-244-3186. Email: dlott@scs.uiuc.edu.

[†] Present address: Department of Chemistry, Chungnam National University, 220 Kung Dong, Yusung Gu, Taejon, 305-764, Korea.

10.1021/jp994153o CCC: $19.00
Published on Web 03/24/2000

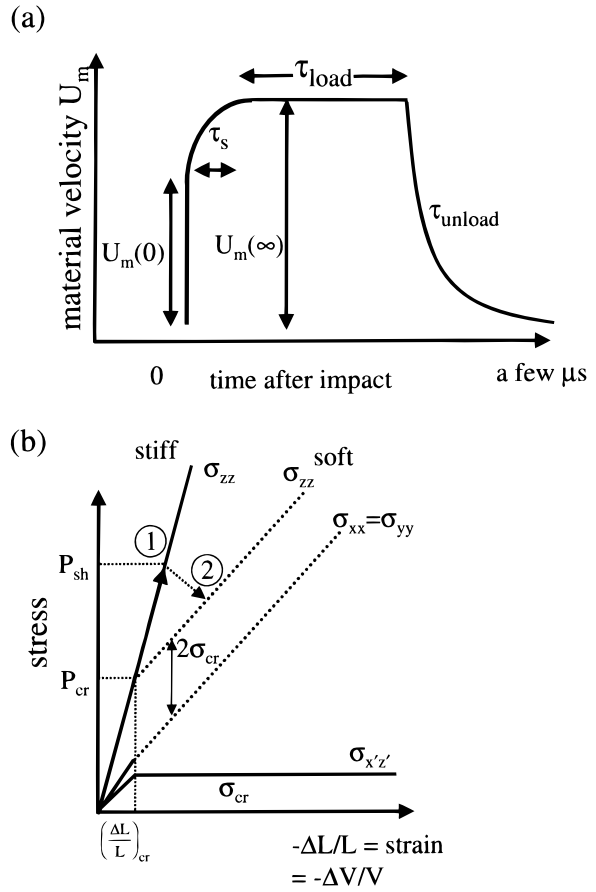

Figure 1. (a) Schematic of the viscoelastic response of PMMA during shock compression measured by velocity interferometry (VISAR). After high velocity impact, there is an instantaneous acceleration to material velocity $U_m(0)$ (the elastic response), followed by a slower acceleration to a final velocity $U_m(\infty)$ (the viscous response) occurring with time constant τ_s. The shock load is held constant for time τ_{load}. (b) Simplified stress−strain diagram. Instantaneous acceleration occurs along the curve for "stiff" polymer, to the point designated "1". A sudden loss of strength occurring with time constant τ_s causes a gradual decay to point "2" along a curve for a "softer" polymer, accompanied by a shear deformation and a second stage of volume compression. σ_{ii} denotes an element of the stress tensor. P_{cr} is the critical pressure where loss of strength occurs and σ_{cr} is the critical shear stress.

response. The second part is a slower viscous relaxation. The two parts are ordinarily described by a constitutive equation involving the bulk modulus K, the shear modulus G, and the viscosity η, referred to as a rheological equation of state.[4,19] In shock compression, viscous relaxation is characterized by a shock viscosity η_{sh},[20,21] so that the strain rate at the shock front is finite.

Continuum viscoelastic models have been used for many years to understand structural relaxation in molecular liquids.[19] More recently, a molecular view of viscoelasticity is beginning to emerge. In molecular liquids, some dynamical processes are believed to consist of a nearly instantaneous inertial motion followed by a slower diffusive relaxation,[22] such as ultrafast polar solvation,[22] optical Kerr effect,[23] photon echoes,[24] or nonpolar solvation in viscous and supercooled liquids.[25,26] In these experiments, the amplitudes of molecular motions are quite small. Berg[25] estimates the pressure change in a nonpolar solvation experiment at about 1 atm, corresponding to a fractional volume change $\Delta V/V_0$ of about 10^{-5}.

Nanoshock experiments[1,2,27,28] involve short duration (∼2 ns) laser-generated shock pulses with very fast rise times (<25 ps). A nanoshock lasts for a few nanoseconds and the shocked sample weighs about one nanogram.[2] The laser which generates the nanoshock is also used to probe the shocked materials using ultrafast molecular spectroscopy, especially coherent anti-Stokes Raman spectroscopy (CARS).[29]

To be specific, consider a typical 4.5 GPa nanoshock in PMMA. High molecular weight PMMA at ambient temperature is a supercooled liquid well below its glass-transition temperature, $T_g \sim 105$ °C, so its viscosity $\eta > 10^{12}$ Pa·s.[7] In the present experiments, the sample is shocked in two stages due to shock reflection from a glass substrate.[30] According to tabulated PMMA shock data,[31] such a two-stage shock[30] to 4.5 GPa shock is produced by an effective impact velocity of ∼0.6 km/s (∼Mach 2). The shock velocity at 4.5 GPa is ∼4 km/s, and volume compression will be about 23%.[31] The shock deposits enough thermal energy to raise the temperature from 25 °C to somewhere in the 125−175 °C range.[16,32] The heating rate is $dT/dt \approx 10^{13}$ K/s. Owing to the micron-scale geometry of our shock target arrays, nanoshocks turn off in just a few nanoseconds[1] when the release wave arrives. A nanoshock load duration is about 10^3 times shorter than in conventional shock compression experiments.[33] That allows us to investigate the effects of very fast unloading processes not previously studied. During unloading, the sample cools at an enormous rate via adiabatic expansion, returning to a temperature slightly above the ambient, estimated at ∼45 °C.[34] The residual temperature increase is due to the irreversible nature of shock compression.[16,35] The cooling rate is $dT/dt \approx 10^{11}$ K/s, which is orders of magnitude faster than cooling by thermal conduction.[2]

Energy landscape models are topographic views of the potential energy function of supercooled liquids used to investigate fundamental phenomena such as melting, arrested kinetics of relaxation, viscosity, and self-diffusion[9] that result from transitions between deep basins in the landscape (α or primary relaxations) or between adjacent local minima within a basin (β or secondary relaxations).[9,36−38] Combining nanoshock experiments with the energy landscape view[6] helps explain the effects of large-amplitude compression and expansion processes in supercooled liquids. The fundamental significance of the present work is the development of an experimental and theoretical framework for producing and probing fast, large-amplitude structural perturbations in supercooled liquids, and for understanding large-amplitude structural dynamics far from the linear response regime. Such a framework might eventually lead to a molecular-level view of high speed impact processes and conceivably to the development of improved impact-resistant materials. Shock waves in medicine also involve large-amplitude dynamics of complex amorphous materials, such as living tissue, which need to be understood at the molecular level. Relevant medical applications include wound trauma induced by projectiles, topical drug delivery by shock waves,[39,40] selective cell killing by laser-generated shock waves,[41] cell poration induced by shock waves, and the effects on biological tissues of shock waves generated in pulsed laser surgery or lithotripsy.

In the rest of this paper, a theoretical section reviews the relevant concepts of viscoelastic and energy landscape models and sets forth the energy landscape picture. A new development in the nanoshock technique is discussed, involving resonance-enhanced excited-state coherent anti-Stokes Raman spectroscopy of a dye molecule probe.[6] Results are presented and discussed for several organic polymers and the protein bovine serum albumin (BSA). These results show how nanoshocks can be used to trigger ultrafast large amplitude structural relaxation

processes which lead to the formation of unique states of large-amplitude compressive or tensile strains.

2. Theoretical Section

Here we discuss the phenomenology of shock compression, we briefly review bulk viscoelastic models and energy landscape models, and then present an energy landscape view of nanoshocks in supercooled liquids.

A. Phenomenology. Conventional shock experiments in PMMA have been reviewed by Schuler and Nunziato.[5] Experimental conditions are chosen to produce nearly planar shock compression.[5,33,35] A uniaxial stress is maintained over the time scale of interest by inertial confinement of the sample in the lateral dimensions. A velocity interferometry technique with time resolution of a few nanoseconds, termed VISAR, has been used extensively.[13,18] A volume element is tagged by the introduction of a thin (150 nm) mirror in the sample. Three regimes are observed. In the low-pressure and high-pressure regimes (said to be $P < 0.8$ GPa and $P > 4$ GPa, respectively),[5] the tagged volume accelerates instantaneously to velocity V_∞ along the direction of shock propagation. In the viscoelastic regime (said to be 0.7 to 4 GPa in PMMA),[5] a two-part response is seen as in Figure 1a. An instantaneous acceleration to velocity $U_m(0)$ is followed by a slower acceleration to $U_m(\infty)$ with time constant τ_s.

An explanation for these observations is now given, based on Chapter XI of ref 35, a classic text in shock compression. This explanation is greatly simplified, but we believe it captures the essential elements. Consider a cylindrical rod of material of length L_0 with pressure P applied to a face. The z-axis is the axis of compression. Ordinarily, compressing a rod causes it to expand or thicken laterally, but in planar shock compression experiments inertial confinement temporarily prevents this. Planar compression is tantamount to either axial compression of a rod encased in a rigid cylinder, or to axial compression of an unconfined rod, followed by lateral compression at constant length back to the original thickness.[35] In planar compression, the fractional length change $\Delta L/L_0$, which is also the fractional volume change $\Delta V/V_0$, is related to the pressure by[35]

$$P = (K + 4G/3)\Delta L/L_0 \tag{1}$$

Equation 1 is of the form stress = modulus × strain. The effective modulus for the confined rod is $M = K + 4G/3$. The bulk modulus K is the fractional change in volume per unit hydrostatic pressure. The shear modulus G, defined in the third part of eq 2 below, describes shape deformation at constant volume. Both K and G depend on a number of factors such as the pressure, the deformation rate, and the deformation path. When a confined rod is compressed by a small pressure P along the z-axis, confinement leads to the development of stresses in other directions. The stress tensor σ is nondiagonal. The nonzero elements[35] are

$$\sigma_{zz} = \left(K + \frac{4}{3}G\right)\frac{\Delta L}{L_0}$$

$$\sigma_{xx} = \sigma_{yy} = \left(K - \frac{2}{3}G\right)\frac{\Delta L}{L_0}$$

$$\sigma_{x'z'} = -\frac{1}{2}(\sigma_{zz} - \sigma_{xx}) = -G\frac{\Delta L}{L_0} \tag{2}$$

The elements of the stress tensor are plotted in Figure 1b. The straight lines in Figure 1b represent more complex curves which are generally concave upward.[35]

As P is increased, the stress tensor continues to obey eq 2 until a critical compressive stress P_{cr} is reached. At P_{cr}, the off-diagonal elements $\sigma_{x'y'}$ reach a critical shear stress σ_{cr}. The critical shear stress characterizes the strength of the material. Above P_{cr} the material undergoes plastic deformation and loses strength. The shear stress will remain pinned at σ_{cr}, as shown in Figure 1b, or perhaps σ_{cr} will increase slightly with P. After plastic deformation begins, the effective modulus M decreases and the material becomes more compressible, as indicated by the sudden decrease in slope of the σ_{zz} curve above P_{cr}.[35]

Returning now to VISAR experiments, in the *low-pressure regime* a strictly elastic response is observed. For a given uniaxial shock load P, the volume instantaneously changes by an amount

$$\Delta L/L_0 = \Delta V/V_0 = P/(K_1 + 4G_1/3) = P/M_1 \tag{3}$$

where M_1 is the effective modulus for this "stiff, elastic" material and K_1 and G_1 are the bulk and shear moduli. After the shock front has passed, the stiff material supports a static shear stress $\sigma_{x'z'}$. The integrity of the lattice is maintained. Graham[33] refers to this situation as the "benign shock paradigm".

In the *high-pressure regime*, where $P \gg \sigma_{cr}$, eq 2 shows that the diagonal elements of the stress tensor become effectively equal and the off-diagonal elements are nearly zero. This situation is usually interpreted to indicate a state of hydrostatic pressure. The immense failure of the lattice due to widespread plastic deformation leads to the generation of a soft, plastic material with fluid-like properties (Graham's catastrophic shock paradigm).[33] For this softer material, the volume change is given approximately (in the limit $P \rightarrow \infty$) by

$$\Delta L/L_0 = \Delta V/V_0 = P/(K_2 + 4G_2/3) = P/M_2 \tag{4}$$

where M_2 is the effective modulus for compressing the soft plastic material, and K_2 and G_2 are its bulk and shear moduli.

Gupta[14] points out that in polymers and other complex materials, the strain rate dependence of the moduli cannot be ignored. Rapid compression to a state characterized by a diagonal stress tensor may differ somewhat from slow hydrostatic compression to the equivalent pressure.

In the *viscoelastic regime*, the shock pressure P_{sh} is only somewhat greater than P_{cr}. The process leading to the two-part VISAR response in Figure 1a is diagrammed in Figure 1b. The first part is an instantaneous uniaxial compression, which is so fast that the material remains stiff. The first part follows a line with slope M_1 to the point labeled "1" in Figure 1b. Now the shear stress is suddenly above σ_{cr}, so the material softens. The softening process occurs with time constant τ_s. As the material softens, further compression occurs, corresponding to the transition from point "1" to "2" in Figure 1b. Only a complex and detailed treatment not done here can say exactly where the point "2" is located. Paradigmatically, at equilibrium the point "2" is located on a hydrostat of the soft material,[35] where $\sigma_{cr} = 0$ and $\sigma_{zz} = \sigma_{xx} = \sigma_{yy}$. In reality, the soft material might retain some shear strength and might equilibrate with a finite shear load. Since the shock duration is finite, the material might not have time to reach equilibrium and point "2" might lie between the stiff compression curve and the hydrostat for the soft material. In polymers, shock induced chemical reactions such as depolymerization or cross-linking might occur as well, causing an additional time-dependence of the material properties. Shock temperature studies by Bloomquist and

Sheffield[42] reported a sudden temperature increase above 1.8 GPa in shocked PMMA, which was attributed to exothermic chemistry.[16]

It is convenient to define a normalized response function $R(t)$, which represents the *time-dependent strain* $\Delta L/L_0$.[25,26] The strain is not always observed directly. In the VISAR experiments,[13,43] the *material velocity* $U_m(t)$ is observed. In shock compression, the strain is the velocity divided by the shock velocity U_s.[31] The shock velocity corresponding to a particular material velocity can be determined if the Hugoniot is known.[31] Hugoniot data are generally given in the form, $U_s = mU_m + b$. For PMMA, linear least-squares fitting to tabulated data[31] gives the result[44] $m = 1.36$ and $b = 2.83$ km/s. A response function can then be defined by using the Hugoniot to convert the time-dependent material velocity $U_m(t)$ into a time-dependent shock front velocity $U_s(t)$, giving

$$R(t) = 1 - \frac{U_m(t)U_s(\infty)}{U_m(\infty)U_s(t)} \tag{5}$$

In eq 5, time $t = 0$ denotes when the shock front reaches the thin mirror, and $U_m(\infty)$ the ultimate material velocity after the shock front has passed.

In Mark Berg's work on nonpolar solvation,[25,26] the response function is derived from measurements of the time-dependent Stokes shift of a probe molecule. The Stokes shift was taken to be proportional to the radial strain. In our experiments, we monitor the passage of a shock front over a polymer doped with dye. Resonance-enhanced CARS[29] is used to measure the intensity and frequency shift of dye vibrational transitions. Electronic and vibrational frequency shifts occur as a result of *density-dependent* changes in intermolecular interactions between the dye and the surrounding polymer. To a good approximation, in the present experiments the frequency shift can be taken as proportional to the *local density change* or *local strain* in the vicinity of the dye probe.[45] For the dye vibrational transition studied here, increased density induces a *vibrational frequency blueshift* $\delta\nu$. The vibrational response function is

$$R(t) = \frac{\delta\nu_{max} - \delta\nu(t)}{\delta\nu_{max}} \tag{6}$$

In the case of dye crystals, the vibrational frequency shift is too small to measure accurately, so we use a somewhat less desirable but easier to measure property, the CARS intensity change. The resonance-enhanced CARS intensity depends on density-induced shifting of electronic transitions in a complicated way, even if the shift is simply linear in the local density, since there may be up to four different changing resonance conditions.[29] The intensity change is thus less straightforward than the vibrational shift. It turns out our lasers are tuned so that the arrival of the shock front causes the CARS intensity to *decrease*. The CARS intensity response function should be

$$R(t) = \frac{I(t) - I_{min}}{|I_{max} - I_{min}|} \tag{7}$$

In eqs 6 and 7, time t denotes the arrival of the shock front at the *front face of the dye−polymer layer*. This point needs discussion. The shock transit time through the VISAR mirror or through our dye−polymer sample, both ~100 nm thick, is about 100 ps. The transit time can be disregarded in VISAR experiments but not in our experiments. The arrival time of the near-IR pulse at the sample is known from optical cross correlation measurements. The shock front arrives at the dye−polymer layer about 1.2 ns later.[1] The shock front arrival varies a few hundred ps from sample to sample, due to slight variations in layer thicknesses. Thus, to determine time zero in $R(t)$, we need to estimate the shock front arrival time at the surface of the dye−polymer sample layer. Judging from the data which will be presented in Figures 6−9, we can do this with an accuracy of about ±20 ps.

B. Viscoelastic Model. The two stages of viscoelastic compression are described by the instantaneous part of the strain $\Delta V_1/V_0$ and the slower part $\Delta V_2/V_0$. After the second stage, the strain is $(\Delta V_1 + \Delta V_2)/V_0$. The simplest form for the viscoelastic strain response is based on the Maxwell model, which gives a two-part function of the form[19,26,46]

$$R(t) = (1 - f)\delta(t) + f[1 - \exp(-t/\tau_s)] \tag{8}$$

where f characterizes the relative amplitude of the two parts

$$f = \frac{\Delta V_2}{\Delta V_1 + \Delta V_2} \tag{9}$$

The δ-function of eq 8 corresponds to the instantaneous elastic response and the second term, including the exponential, corresponds to the slower viscous response. For polymer and protein relaxation a stretched exponential[7] might be a better choice for eq 8, but an exponential approximation is good enough for shock experiments, where measurements are made over a limited range of time. As mentioned in the discussion of Figure 1b, the two stages of volume relaxation described by eq 8 involve both bulk and shear moduli of the stiff and soft polymer. A detailed microscopic treatment of polymer volume relaxation not done here is needed to find the exact relationships between these moduli and the volume changes ΔV_1 and ΔV_2. However, the bulk and shear moduli obtained by such a treatment would certainly be of the same order of magnitude as the tabulated values of the *static* bulk and shear moduli.

The relaxation time τ_s in this model is[19]

$$\tau_s = \eta_{sh}/M_2 \tag{10}$$

where M_2 is the effective modulus for compression of the soft material in the second stage and η_{sh} is an effective coefficient of viscosity under shock conditions, the "shock viscosity".[20,21]

The shock viscosity concept[20,21] was introduced to account for the finite rise times of shock fronts in solids. The shock viscosity η_{sh} describes dissipative effects which limit the rates of shear deformation and volume compression in the second stage of compression.[20,21] *The shock viscosity tells us the strain rate at a given stress*. This shock viscosity differs from ordinary coefficients of viscosity which describe the behavior of fluids or supercooled liquids under the influences of weak perturbations. For example, the zero-frequency viscosity describes fluid flow under a weak perturbation such as gravity, and the infinite frequency viscosity τ_∞ describes dissipative effects such as high-frequency acoustic attenuation,[19] where the perturbation is again small. A viscous liquid flows through a pipe under the influence of gravity. A solid will also flow through a pipe if it is shocked with enough force to produce a large plastic deformation. For example, Prieto and Renero[20] analyzed VISAR rise time measurements of shock waves in aluminum[47] to determine the shock viscosity of aluminum slabs. They found a shock viscosity for *solid aluminum* at 4 GPa of only 140 Pa·s. In other words, with a great enough shock load, solid metal can flow with the viscosity of a heavy sugar syrup.

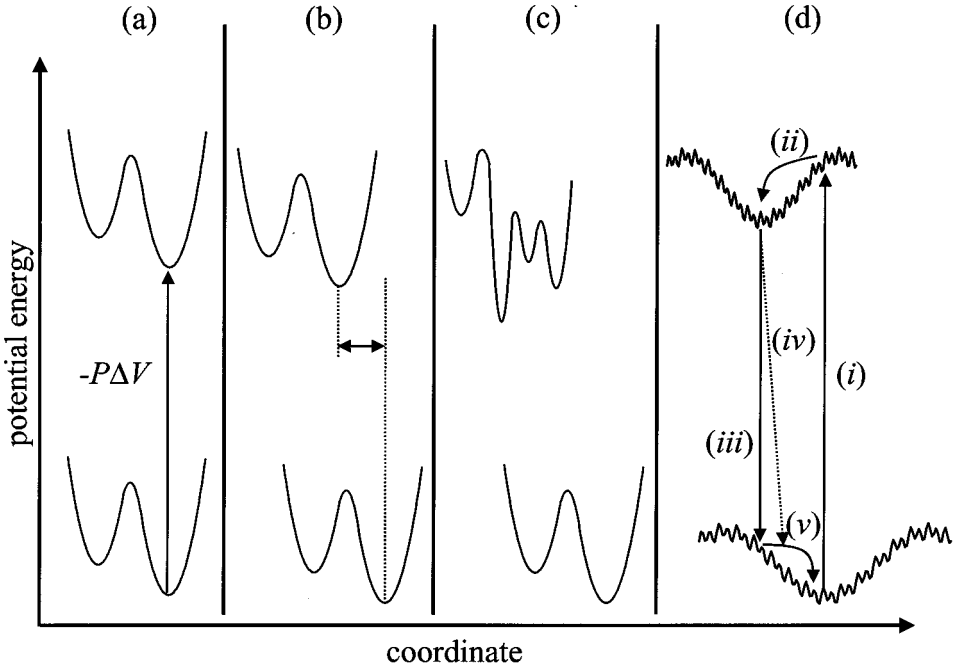

Figure 2. Energy landscape model. (a−c) The effects of compression on a small section of the energy landscape as a function of any coordinate other than the volume coordinate R. (a) Compression (reducing R) raises every state by an energy $-P\Delta V$. (b) The potential minima are displaced. (c) New minima and new barriers are created. (d) Dynamic shock compression on an energy landscape. An instantaneous compression results in a sudden jump (*i*) to a new region of the landscape where the topography for motion along every coordinate is suddenly altered. (*ii*) Large-amplitude structural relaxation on the shocked landscape following sudden compression. (*iii*) Hypothetical path for instantaneous expansion shock unloading. (*iv*) Tilted path for slower expansion where some structural relaxation occurs during unloading. (*v*) Large-amplitude structural relaxation on the ambient landscape following a nanoshock cycle of compression and expansion.

C. Energy Landscapes and Shock Waves. In a supercooled liquid with N-atoms, the potential energy function is $\Phi(r_1, r_2, ..., r_N)$. The potential energy topography or "landscape" for motion along any configurational coordinate consists of several deep basins separated by barriers.[9] Each basin is characterized by a rugged structure with many local minima.[9,36−38] The idea of a rugged potential energy landscape helps explain many of the unique properties of supercooled liquids.[9] The landscape view ought to be useful as well for understanding static or dynamic high-pressure experiments on supercooled liquids or proteins,[48] or dynamic shock compression experiments,[6] but it has not been used much so far in this context.

Consider an N-particle potential function $\Phi^\circ(r_1, r_2, ..., r_N)$ defining the system at low pressure. Transform the coordinates to create a size coordinate R so that the potential function is expressed as $\Phi^\circ(R, r_1, r_2, ..., r_{N-1})$, where the r's are orthogonal to R. When pressure is applied to a system with an *entirely harmonic surface*, the landscape changes to

$$\Phi(R', q_1, ..., q_{N-1}) = \Phi^\circ(R, q_1, ..., q_{N-1}) - P\Delta V \quad (11)$$

where in compression, $R - R' > 0$. Equation 11 shows that the potential energy of every configuration in a harmonic material is simply increased by the work done on the system $-P\Delta V$. The topography for motion along any coordinate q_i is unchanged for compression of a harmonic lattice.

In a real anharmonic solid, the series expansion for Φ includes higher order terms that cannot be neglected when $R - R'$ is not small.[49,50] In particular, consider terms of the form

$$\left.\frac{\partial^2\Phi^\circ}{\partial R \partial q_i}\right|_{R_0,q_0} (R - R') \quad (12)$$

and

$$\left.\frac{\partial^3\Phi^\circ}{\partial R \partial^2 q_i}\right|_{R_0,q_0} (R - R') \quad (13)$$

Equation 12 shows that the locations of *minima* in the potential surface are functions of R. Similarly, eq 13 shows that the *curvature* of the potential surface is a function of R. Thus compression (increasing $R - R'$) or expansion (decreasing $R - R'$) can dramatically affect the landscape for motion along any coordinate q_i. In compression, the basins corresponding to stable structures move to different regions of configuration space. New basins may be created and old basins may be destroyed. Similarly the barriers between configurations may become higher or lower. Since the curvature generally increases with increasing density, the number and steepness of barriers will generally increase as well. Molecular dynamics simulations of supercooled liquids with anharmonic potential energy surfaces show that inherent structures corresponding to local minima exist only for limited volume ranges.[51,52] The effects of compression on a small region of the potential surface of an anharmonic supercooled liquid are illustrated schematically in Figure 2. Figure 2a shows that compression raises the potential energy by $-P\Delta V$. Figure 2b shows that terms such as the one in eq 12, one of many terms in the potential expansion that contributes to the Grüneisen parameter,[49,50] result in a displacement of potential minima along the coordinate q_i. Figure 2c shows that terms such as eq 13 can give rise to new barriers and new local minima for motion along coordinate q_i.

To illustrate, consider structures associated with the conformations of a methyl rotator. At very low density, a methyl rotator may be a free rotor. As the density is increased, barriers to motion along the rotation coordinate appear and the familiar three-well structure may form. As compression continues, new barriers to rotation will be created, and the deep wells of stability will move around or even disappear. In this example, compres-

sion causes the topography for methyl rotation to evolve from a relatively flat surface to a three-well surface to a rugged surface with a large number of local minima.

Let us consider the effects of dynamic compression or expansion on an anharmonic supercooled liquid. First consider reversible expansion or compression. A reversible process is one that occurs much slower than the accompanying structural relaxation. As the density (*R*-coordinate) is changed, the system gradually moves to a new region of the energy landscape where the topography for motion along any coordinate q_i becomes quite different, and where the structure of the most stable conformations is also quite different. Slowly increasing or decreasing the density thus causes a gradual evolution of the system's structure and the topography of the landscape for motion along the coordinates q_i.[6]

Now consider the effects of shock compression by an instantaneously rising shock front (a limiting case). A strong shock causes a sudden inertial motion along the *R*-coordinate, resulting in a radical change in the topography for motion along any coordinate q_i.[6] This inertial motion primarily involves decreasing the distances between nonbonded atom pairs. Covalently bonded atom pairs are much more difficult to compress.[53] In instantaneous shock compression, the inertial motion occurs on a time scale of a few tens of fs, roughly the time needed to move the atom pairs at the speed of sound (a few angstroms per picosecond). During this very fast inertial phase there is no time for the system to surmount the barriers that separate adjacent local minima, so coordinates other than *R* do not have time to change during the initial phase of shock compression. As illustrated in Figure 2d, instantaneous shock compression may be viewed as a sudden vertical transition to a new region of the energy landscape,[6] which we will term the "shocked" or "compressed" landscape. The transition is vertical in the sense that the inertial change in the *R*-coordinate is much faster than structural evolution along the q_i coordinates. In this new region of the energy landscape, the topography for motion along coordinates q_i is very different. The initial configuration is unstable—quite likely highly unstable. As illustrated in Figure 2d, the unstable configuration will subsequently undergo structural relaxation in the new region of the energy landscape. This view of shock compression of amorphous materials as a vertical transition to a new region of the landscape is new, and it is a useful way of understanding the effects of shock compression in amorphous materials.[6]

An instantaneous expansion (another limiting case) may similarly be viewed as a vertical transition downward from the compressed landscape to the ambient landscape, as in Figure 2d. Instantaneous expansions and absolutely vertical downward transitions are not theoretically obtainable.[35] An instantaneous expansion shock front would cause a spontaneous decrease in entropy forbidden by the Second Law of Thermodynamics. Thus, real shock unloading processes should be viewed as being slower than instantaneous but much faster than a slow reversible expansion. A reversible expansion would follow a tilted path that would return the system to a configuration near the global minimum of the deep basin. The shock unloading process follows the dashed arrow in Figure 2d, a path that is tilted somewhat toward the bottom of the deep basin. The magnitude of the tilt represents the extent of structural relaxation that occurs during the unloading process.

The vertical transition between landscapes is reminiscent of and analogous to the Born−Oppenheimer principle for molecular electronic transitions. The Born−Oppenheimer principle is approximately valid because the mass of the electron is much less than the mass of a nucleus. The vertical shock transition model is approximately valid because the periods of intramolecular and intermolecular vibrations of molecules in supercooled liquids are much smaller than the times needed to go over the barriers separating different conformational states.

The two-part viscoelastic response to shock is a natural consequence of the shock energy landscape model. After a vertical transition to a shocked energy landscape, the system (Figure 2d, (*i*)) finds itself in an unfavorable configuration. It will then undergo structural relaxation over barriers on the shocked landscape toward the bottom of the basin (Figure 2d, (*ii*)), to release the excess energy stored in conformational coordinates (excess strain energy). This dynamical relaxation is analogous to the internal conversion process which causes the Stokes shift in fluorescence. Relaxation on the shocked landscape may be very fast because the temperature is elevated and the shock viscosity may be orders of magnitude smaller than the ambient viscosity. A transition from a shocked landscape to the ambient landscape via rapid expansion (Figure 2d, (*iii*) and (*iv*)) would leave the system high up on the ambient potential energy landscape, where it might undergo further structural relaxation toward the global minimum (Figure 2d, (*v*)). These last two processes (*iv*) and (*v*) are very interesting because, provided that structural relaxation process (*v*) is slow or improbable, process (*iv*) will produce highly distorted structures with large-amplitude compressive strain, such as "densified materials",[11] or possibly unique combinations of compressive and tensile strains (vide infra). Using short duration nanoshock pulses to produce these large amplitude states would permit the systematic study of structural relaxation dynamics on the ambient landscape far from the small-amplitude, linear response regime studied by conventional techniques.

3. Experimental Section

A. Nanoshock Technique. The nanoshock technique has been described previously,[1,2] but the use of resonance CARS probing is new. A brief sketch of the experiment is shown in Figure 3 (top). A large area (~100 cm^2) multilayer shock target array is fabricated on a glass substrate. The top layer, termed the "shock layer", consists of PMMA doped with a near-IR absorbing dye. A near-IR Nd:YLF laser pulse ($\lambda = 1.053$ μm, 80 ps duration, ~100 μm diameter, 320 μJ energy unless otherwise indicated) generates a nanoshock by laser ablation of the shock layer. The shock front propagates through an impedance-matched buffer layer several μm thick. When the front emerges from the buffer layer, it is as if a tiny (~100 μm diameter) ram smashed into the sample[32] at a velocity of ~0.6 km/s. The shock layer ablates away while the shock front is delayed in the buffer layer.[30] After the shock layer debris plume has dissipated, in about 1 ns,[30] time-delayed probe pulses from two synchronously pumped dye lasers (25 ps duration, ~10 μJ energy) interrogate a small region (~20 μm diameter)[30] in the center of the shocked volume. Every time a shock is generated, the sample is destroyed. The array is translated by a motorized positioner to present a fresh sample to the laser on every shot. Spectra are obtained by signal averaging a few thousand shots at a repetition rate of 80 Hz.

Although the nanoshock is generated from a laser pulse with a Gaussian profile and it expands in a spherical geometry, in the central region (~20 μm diameter) interrogated by the probe pulses (Figure 3), the nanoshock front travels at a nearly constant velocity and it produces a nearly planar compression over the first ~10 nanoseconds of travel.[2,30] The shock has a rise time (10−90%) <25 ps and a fall time (10−90%) of 2 ns.[1,2,27] The

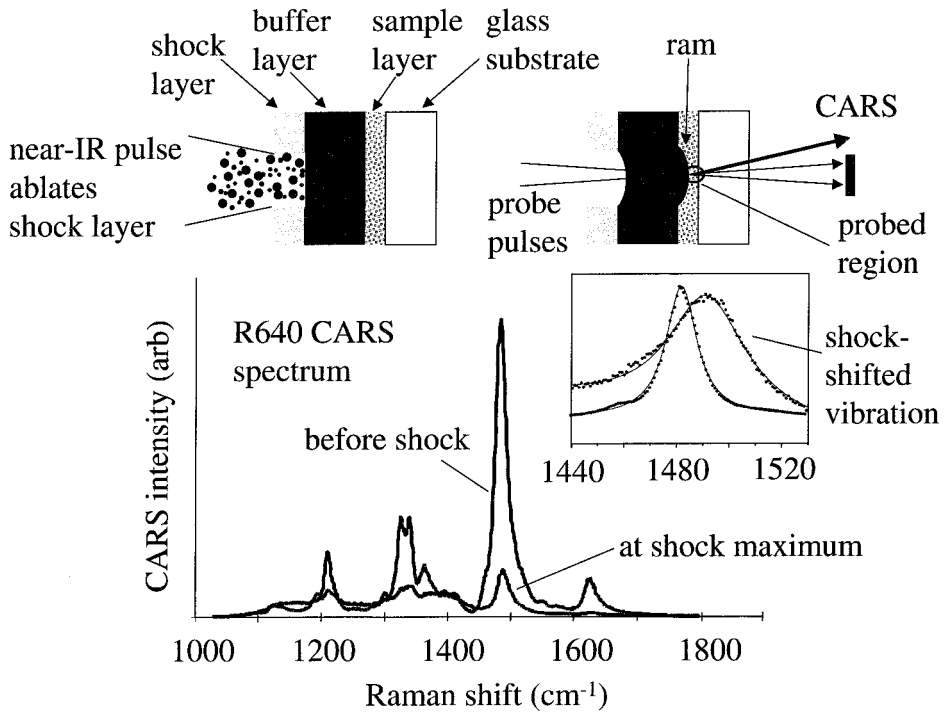

Figure 3. (top) Schematic diagram of the nanoshock experiment. The near-IR laser pulse launches a shock into a shock target array, which can be viewed as impact by a tiny (∼100 μm diameter) ram on the thin (∼100 nm) sample layer. In the ∼20 μm diameter region probed by laser pulses at the center of the ram, shock compression appears almost planar for the first several ns. After each nanoshock, the sample is translated to a fresh spot. The vibrational spectrum of a dye in the sample layer is monitored by resonance CARS spectroscopy. (bottom) Resonance CARS spectrum of R640 dye in PMMA prior to and just after shock. (inset) The most intense vibrational transition at ∼1480 cm^{-1} is fit by a Lorentzian function (solid curve) to extract the shock-induced frequency shift. Reproduced from ref 6, ©1999, American Physical Society.

sample layer sees a two-stage shock due to a shock reflection from the adjacent glass substrate. The pressure rise in the second stage is about two-thirds of the first stage.[30,34] The time resolution in the experiment is limited primarily on the shock round-trip transit time through the sample.[30,34] For a typical 100−200 nm thick sample (200−400 nm round trip) and a shock velocity of 4 km/s, the time resolution is 50−100 ps. Similar two-stage shocks in anthracene, a model system used to study the properties of nanoshocks,[1] have a pressure[34] of $P = 4.7$ (±0.2) GPa (in two steps, 0 → 2.9 and 2.9 GPa → 4.7 GPa). That should also be a reasonable estimate for the shock pressure in our polymer experiments. However, the actual shock load depends on day-to-day variations in experimental conditions and the samples' shock impedances,[31] which are not accurately known except for PMMA. We believe the actual shock pressure is within 10% of 4.7 GPa, and therefore cite a 4.5 GPa value, keeping in mind that it is supposed to indicate a 4−5 GPa range.

B. Resonance Excited-State CARS Probe. Broad-band multiplex nonresonant CARS spectroscopy[29] was used in our earlier nanoshock experiments.[2,28] The higher frequency probe pulse has a narrow bandwidth (∼1.5 cm^{-1}) which determines the spectroscopic resolution, and the lower frequency pulse has a broad (here ∼350 cm^{-1} fwhm) bandwidth, which determines the width of the probed spectral range. The signal is detected with a spectrograph and a charge-coupled detector array. It is problematic to obtain good CARS signals from a 100 nm thick partially dye-doped layer. Even conventional resonance-enhanced CARS is not good enough. In nonresonant experiments, we ordinarily use a probe intensity of ∼30 GW/cm^2, just below the single-shot damage threshold. When laser power is effectively unlimited, as is the case with our setup, the resonance CARS sensitivity is limited by the saturation intensity of the resonant electronic transition.[29] The saturation intensity

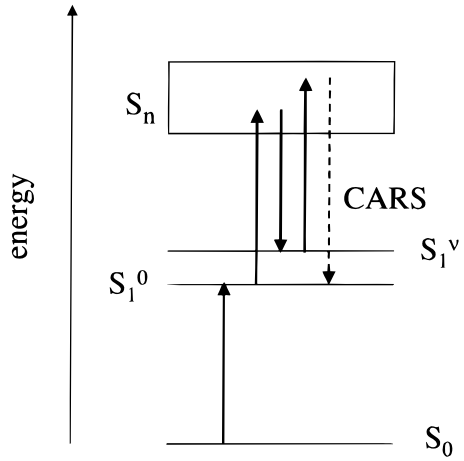

Figure 4. Energy level diagram for resonance excited-state CARS. The leading edge of the probe pulse drives dye molecules into the first excited singlet state S_1. Then the CARS intensities of vibrational transitions of S_1, of the form $S_1^0 \rightarrow S_1^v$, are enhanced by resonance with the $S_1 \rightarrow S_n$ transition. Larger laser intensities can be used and larger CARS signals can be obtained with excited-state CARS because the S_n state relaxes back to S_1 much faster than S_1 relaxes back to S_0.

$I_s = h\nu/\sigma\tau$, where σ is the cross-section and τ the excited-state lifetime. For the $S_0 \rightarrow S_1$ transition of the dyes used here, $\sigma \sim 2 \times 10^{-16}$ cm^2 and $\tau \sim 5$ ns, so $I_s \sim 0.3$ GW/cm^2. A probe intensity below 0.3 GW/cm^2, which is 100 times less than we usually use, results in a small CARS signal. To overcome this problem, we use resonance enhancement of an *excited-state transition*, denoted $S_1 \rightarrow S_n$,[54] as shown in Figure 4. A very small part (∼1% of the total energy) of the leading edge of the probe pulse drives the dye to the first singlet state S_1. The rest of the probe pulse generates the CARS spectrum of vibrational transitions in the S_1 state, of the form $S_1^0 \rightarrow S_1^v$, resonantly

enhanced by the $S_1 \rightarrow S_n$ transition. The lifetime of S_n is very short, probably just a few picoseconds,[54] so the saturation intensity of the $S_1 \rightarrow S_n$ transition is about 10^3 times greater than for the $S_0 \rightarrow S_1$ transition. Then even 30 GW/cm^2 pulses can be used which do not saturate the transition, resulting in an extremely sensitive probing technique.

We used the dyes Rhodamine 640 (R640) or sulforhodamine 640 (sR640, a water-soluble version of R640), from Exciton Chemical. These dyes have similar absorption and CARS spectra. Even the $S_1 \rightarrow S_n$ spectra are similar.[54] An example of a resonance CARS spectrum is shown in Figure 2 for R640 in 100 nm thick PMMA. Each spectrum is the average of ~8000 shots. The spectra are not corrected for the system spectral response, which has a peak near 1500 cm^{-1} and a fwhm of about 350 cm^{-1}.

The most intense vibrational transition of the dyes, at ~1480 cm^{-1}, is used as a probe of local structural dynamics in the same way that time-dependent dye spectra have been used to probe structural evolution in polymers and glasses,[55] or solvation dynamics of liquids and glasses.[22,23,25,26,56−58] Shock loading causes this vibrational transition to blue shift and broaden. A computer is used to generate a Lorentzian fit to the line shape, as shown in the inset. The maximum blue shift for the 4.5 GPa shock is 10 cm^{-1}. Since there is one data point every 0.8 cm^{-1}, and there are tens of data points in every fitted curve, peak shifts as small as ~1 cm^{-1} can be accurately determined.

C. Sample Preparation. Five polymers and one crystalline sample were used: (1) high molecular weight PMMA (average MW ~ 1 000 000); (2) low molecular weight PMMA (average MW ~ 15 000); (3) poly(vinyl alcohol) (PVA, 99% hydrolyzed, average MW 150 000,); (4) poly(ethylene oxide) (PEO, average MW ~ 4 000 000); (5) bovine serum albumin (BSA, 98−99% lyophilized powder); and (6) polycrystalline sR640. The polymers were purchased from Aldrich, the BSA from Sigma, and the dyes from Exciton.

As shown in Figure 3, the shock target arrays have a four-layer structure, consisting of a 3 mm float glass substrate, and then a series of layers with about the same shock impedances: a 100−300 nm thick sample layer, a nominally 5 μm thick PVA buffer layer, and a 2 μm thick shock layer (PMMA plus IR-165 dye). Recipes for most of these layers have been published previously.[30] The main issue is that the solution used to coat a given layer should not dissolve the layer underneath.[2] For water-insoluble samples such as PMMA, the buffer layer was PVA deposited from aqueous solution.[30] For water-soluble layers, a thin (0.3 μm) protective coating of PMMA was used before the PVA was applied.[59]

The PMMA samples were applied by spin coating PMMA and R640 dye in a mixture of ketones. The dye absorbance was about unity at 580 nm, corresponding to ~5% dye by weight. The PMMA thickness was less than 200 nm, as measured by a Dektak profilometer. The PMMA was cured in an oven below T_g for 1 or 2 h, which prevented the dye from leaching into the solution used to coat the buffer layer. A 5 μm PVA buffer layer and the shock layer were subsequently added.

The PVA, PEO, and BSA samples were coated from aqueous solutions containing water-soluble sR640 dye. The BSA sample is intended to be a very crude model for a dry biological tissue. It was prepared by spin coating 5 mL of pH 7 phosphate buffer containing 6 mg of sR640 and 300 mg of BSA at 600 rpm for 25 s. The BSA layer was ~0.3 μm thick, and it was not as smooth and flat as the organic polymers. The PMMA coating, the PVA buffer layer, and the shock generation layer were then applied to these water-soluble samples.

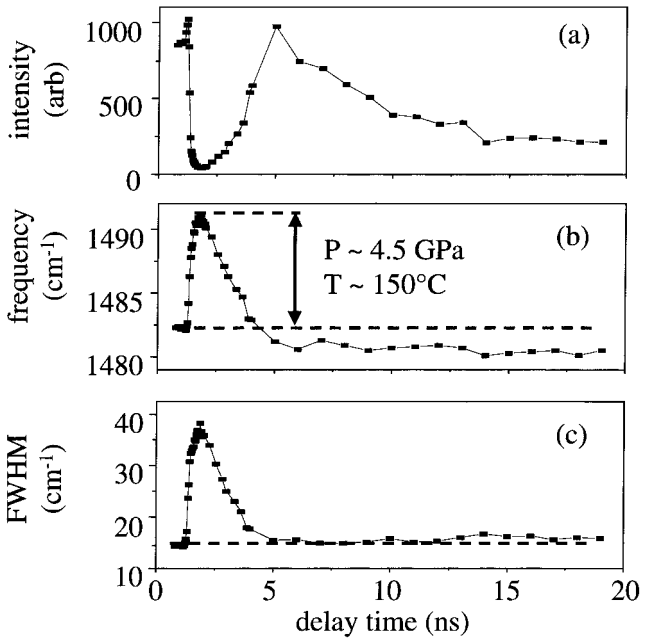

Figure 5. Data for the ~1480 cm^{-1} R640 vibrational transition in PMMA with a 4.5 GPa nanoshock pulse. (a) CARS intensity. The intensity decline for $t > 5$ ns is due to shock-induced CARS signal deflection by the buffer layer. (b) Frequency shift. (c) Line width. Reproduced from ref 6, ©1999, American Physical Society.

A sample of pure polycrystalline sR640 dye was prepared by spraying an aerosol solution of sR640 in methanol:dichloromethane onto the glass substrate with an air brush.[30] The dye layer thickness was optimized to produce the desired absorbance of unity at 580 nm, which turned out to correspond to <100 nm thickness. The polycrystalline dye layer had an irregular topography. The subsequent layers were applied to the water-soluble dye as above.

4. Results

A. Intensity, Shift, and Width. Figure 5 shows results over the time range of 0−20 ns for the ~1480 cm^{-1} vibrational transition of R640 in high molecular weight PMMA with a 4.5 GPa shock. When the shock front reaches the sample, there is a sudden CARS intensity drop (Figure 5a), a sudden blue shift (Figure 5b), and a sudden broadening (Figure 5c). The sudden intensity drop is caused by pressure detuning of the resonance CARS effect. The width increase is attributed to the shock-induced temperature increase, although a contribution from a small pressure gradient across the probed volume cannot be ruled out. The intensity and width recover over the next few nanoseconds as the nanoshock unloads. The shift recovers and overshoots, becoming frozen at ~2 cm^{-1} to the red of its original position (i.e., a blue shift of −2 cm^{-1}). After the intensity recovers at $t \approx 5$ ns, it decreases again over the next 10 ns. This slower intensity change is not associated with molecular dynamics of the sample. It results from CARS signal beam deflection away from the entrance slit of the spectrograph due to shock ringing in the buffer layer. The deflection can be seen by eye. The shift and width measurements are insensitive to intensity variations, so we view them as more reliable in the >5 ns time range. Using the width and shift, we can better investigate the state of the samples after the nanoshock pulse is over.

B. Crystalline Dye. Figure 6a shows the short-time behavior of the intensity response function $R(t)$ for the polycrystalline layer of sR640 dye, computed from the data using eq 6. The

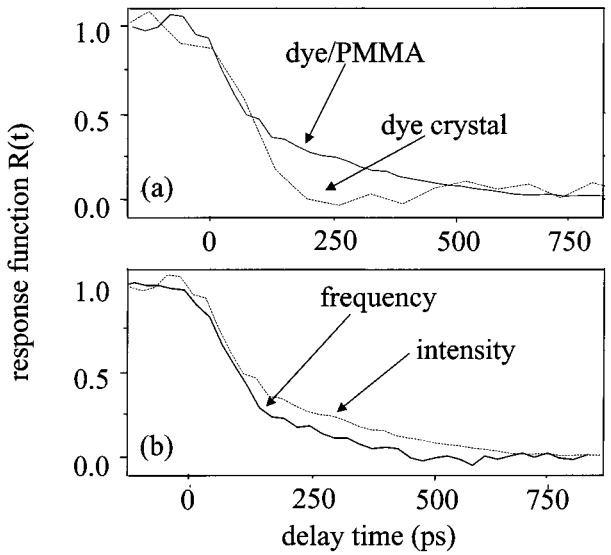

Figure 6. (a) Intensity response function with a 4.5 GPa nanoshock for crystalline sR640 dye and R640 dye in PMMA. Time zero denotes the arrival of the shock front at the sample layer. The dye crystals show only an instantaneous response, limited by the ~110 ps shock round trip time in the sample. The polymer shows the instantaneous part plus a slower ~300 ps part not observed in crystals. (b) Frequency shift and intensity response functions for R640 in PMMA. The frequency shift is approximately proportional to the local density near the dye probe. The intensity change is more complicated, involving density-dependent pressure shifting of the four resonances involved in generating the CARS signal.

intensity response is used here because the vibrational frequency shift is very small. The onset of the intensity drop is used to define $t = 0$. The intensity fall time (90%−10%) is 110 (±10) ps, exactly what would be expected for a shock round trip through the dye layer. The polycrystalline dye results are consistent with an essentially instantaneous material response limited by the shock round trip time. An instantaneous response has previously been seen in polycrystalline anthracene samples.[1,27]

C. Dye in PMMA. The intensity response of R640 dye in PMMA is compared to the sR640 dye crystal data in Figure 6a. The two $R(t)$ curves are slightly offset in time to account for a slightly different shock arrival time. In PMMA, $R(t)$ has a characteristic two-part structure. There is an instantaneous drop followed by a slower decay of similar amplitude. This slower response has not been observed in previous nanoshock experiments on crystalline materials,[1,27] only now with polymers and proteins.

Figure 6b compares the vibrational shift and intensity response of R640 in PMMA. Both have the same two-part structure, but the relative amplitudes of the two parts are a bit different. As mentioned above, the shift is more straightforward to relate to the strain, so from now on we will discuss only shift data. The total shock-induced frequency shift for R640 in PMMA is ~10 cm^{-1}; the amplitude of each of the two parts is ~5 cm^{-1}.

D. Other Polymers. Figure 7 compares the frequency shift response for R640 in high molecular weight PMMA to dyes in the other polymer samples. Essentially the same response is observed for all: high molecular weight PMMA; low molecular weight PMMA, PVA, PEO, and BSA. The longer time data (>1 ns; not shown) are the same as what is seen for PMMA in Figure 5.

E. Dependence on Shock Pressure. The dependence on shock pressure was studied in high molecular weight PMMA. The shock pressure was varied by attenuating the near-IR shock generation pulse. The data in Figure 8 were obtained with 240, 320, and 400 μJ pulses (320 μJ pulses were used in all of the other experiments). At a rough guess based on earlier work, which shows the shock pressure starts to saturate near 320 μJ, these correspond to shock pressures of 3.5, 4.5, and 5 GPa. As the shock pressure is increased the shock front arrives a bit sooner, and the faster part of the response speeds up because the shock velocity increases. The different arrival times in Figure 8 should be regarded as significant, since identical samples were used and only the laser intensity was varied. The slower part of the response function becomes systematically faster as the shock pressure is increased. It is easiest to see this in the intensity

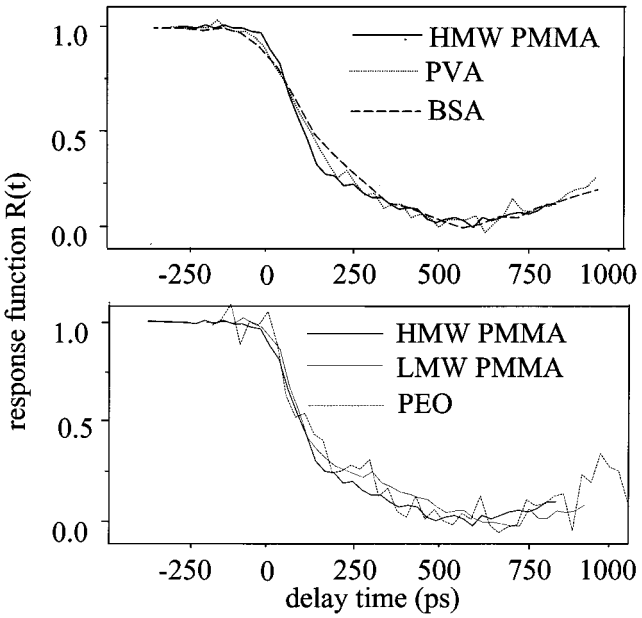

Figure 7. Frequency response functions with a 4.5 GPa nanoshock for different polymers: HMW PMMA = high-molecular weight PMMA. LMW PMMA = lower-molecular weight PMMA. PVA = poly(vinyl alcohol). BSA = dried film of bovine serum albumin. PEO = poly(ethylene oxide).

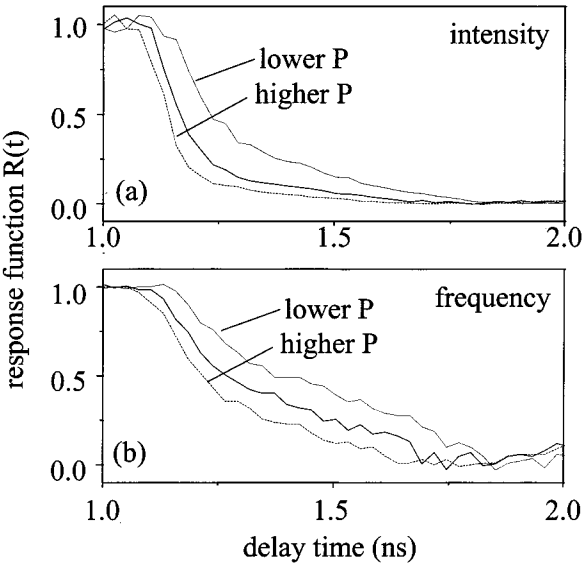

Figure 8. Intensity (top) and frequency shift (bottom) response functions for R640 dye in PMMA with nanoshock pressures in the 3.5 to 5 GPa range. At higher shock pressures, the shock arrives sooner and the decay is faster. Increasing the shock pressure decreases the time constant τ_s for the slower relaxation process but it has little effect on the f-parameter in eq 8, which characterizes the relative amplitudes of the faster and slower processes.

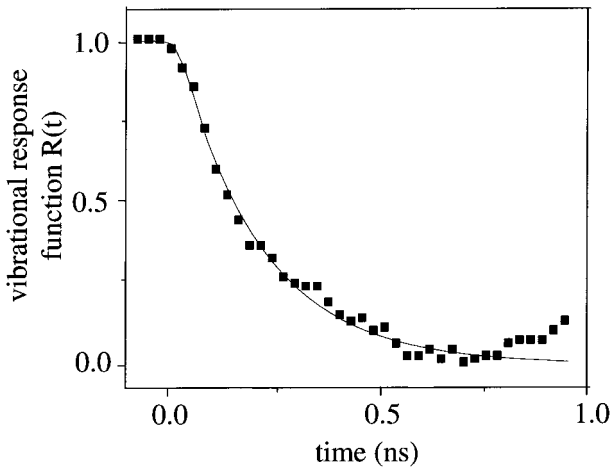

Figure 9. Vibrational frequency shift response function for R640 in PMMA with a 4.5 GPa nanoshock fit to eq 8 (solid curve). The data begin to turn up after 0.75 ns as the nanoshock starts to unload. Unloading is not considered in the model.

response data in Figure 8a, but careful examination shows it also happens in the frequency shift data.

F. Viscoelastic Model. The PMMA frequency shift data were fit to the viscoelastic model of eq 8. The model was modified to account for the finite propagation time of the shock front across the sample by convolving eq 8 with an apparatus response function. This function starts at time zero and ends at 110 ps. It rises linearly with a slope, given by the average shock velocity, to represent the shock front double-passing the sample.[30] Figure 9 shows that the fit to the PMMA data is very good. Notice that the data start to turn back up at about 0.75 ns due to nanoshock unloading, but that the fitted curve does not turn up because the effects of unloading were not incorporated into the model. The fit parameters for PMMA were $f = 0.48 \pm 0.04$ and $\tau_s = 150 \pm 50$ ps. Essentially the same values were obtained for the other organic polymers and BSA. The cited error bounds have little to do with the goodness of fit or scatter in the data points. They reflect our uncertainty in knowing the precise shape of the nanoshock pulse. We do not know exactly how much relaxation occurs during the ~100 ps shock transit time, and we do not know precisely when the nanoshock starts unloading. Using the viscoelastic model with the pressure-dependent PMMA data in Figure 8, we find that f does not change much with pressure (in the 3.5−5 GPa range) but τ_s decreases with increasing pressure in this same range.

We can estimate the shock viscosity as follows. For PMMA with a 4.5 GPa shock, the volume change $\Delta V/V = 0.23$.[31] At this pressure, the corresponding modulus is M_2, the modulus for compressing the "softer" PMMA, so eq 4 gives $M = 19.2$ GPa. For a time constant $\tau_s = 150$ ps, eq 10 yields a viscosity $\eta_{sh} \approx 3$ Pa·s. For comparison, this viscosity is about the viscosity of glycerol at 15 °C. Notice that this value of η_{sh} refers to the specific conditions produced by nanoshock compression.

The data in Figure 8 may be used to draw some qualitative conclusions about the dependence of η_{sh} on shock pressure in the range studied here. Since M_2 increases only slightly (<20%) in this pressure range,[31] the decrease in τ_{sh} with increasing pressure in Figure 8 is primarily due to a decrease in η_{sh} with increasing pressure.

5. Discussion

A. Review. The steeply rising shock front in PMMA jumps the pressure to ~4.5 GPa and the temperature to ~150 °C. Shock tables tell us that 4.5 GPa in PMMA produces a volume compression[31] $\Delta V/V_0 \approx 0.23$. All of the organic polymers and the BSA showed a similar two-part response: an initial instantaneous part and a subsequent slower (viscous) response occurring over ~300 ps (i.e., twice the exponential time constant of 150 ps). The two parts had roughly equal amplitudes, that is $f \approx 0.5$ in eq 8. For $f = 0.48$ (the value observed for PMMA), the volume compression in the first stage $\Delta V_1/V_0 \approx 0.12$, and in the second stage $\Delta V_2/V_0 \approx 0.11$. The final density $\rho_f = \rho_0[1 - (\Delta V_1 + \Delta V_2)/V_0]^{-1} \approx 1.3\ \rho_0$. The effective shock viscosity for the slower response was quite small, just a few Pa·s. Limited pressure-dependent data shows the viscosity decreases a bit (perhaps by a factor of 2−3) as the shock pressure was raised from 3.5 to 5 GPa. The dye frequency blue shift increases by about 5 cm^{-1} in each of the two stages of compression. During the ~4 ns unloading process (i.e., twice the 2 ns fall time), the dye red shifts by ~12 cm^{-1}, to a blue shift of about −2 cm^{-1} (i.e., a red shift of 2 cm^{-1}), where it remains frozen for at least 20 ns. For the purposes of further discussion, we will estimate the pressure corresponding to this unique state as follows. We make the reasonable ansatz that the dye blue shift is proportional to the local density increase, and a cruder approximation that the pressure is also proportional to the density increase. Then the −2 cm^{-1} blue shift indicates a *negative pressure*, equal to about one-fifth of 4.5 GPa, or about 1 GPa.

B. Crystals vs Polymers. Because all of the polymer samples evidence nearly identical response to the shock front, we ought to be concerned that the response is determined by the apparatus rather than by the sample. Earlier, [27] we studied polycrystalline layers of anthracene 0.7 μm thick. The shock transit time was 180 ps. No evidence for a slower second-stage viscoelastic response was observed; all of the shock front dynamics were complete in 180 ps. In anthracene, the CARS transition studied was quite sharp (fwhm = 4 cm^{-1}). When a steep front was inside the anthracene layer, the CARS spectrum was split into two peaks representing material ahead of and behind the front.[27] By analyzing this splitting, we were able to determine that the shock front rise time, $t_r < 25$ ps, was even less than the 180 ps transit time. The anthracene layer thus showed an essentially instantaneous shock response characteristic of a nonviscous fluid. The conventional explanation for fluid-like behavior of crystalline solids is that for shock pressures above a critical stress, termed the Hugoniot elastic limit,[33] massive destruction of brittle crystals occurs in the shock front.

The present results indicate a similar fluid-like response for the brittle dye crystals, in that the 110 ps response time of the dye layer is that expected for a sample whose response was solely limited by the shock front round trip time. Although the dye CARS transition being monitored is too broad to resolve any two-peak structure, we can still say that the shock front rise time cannot be much greater than ~50 ps, otherwise the fast part of the shock front response would be noticeably affected.

The dye crystal data show that the apparatus response time is <110 ps, where the "apparatus" is the laser system plus the various layers that comprise the shock target array. The polymer and protein samples show a long tail that persists for about 300 ps. Polymer samples show a shock response that is slower than anthracene, even though the polymer sample is thinner than the anthracene sample. Thus, the slower response of the polymer and protein layers cannot be instrument limited.

C. Conceptual Model of Viscoelasticity. A conceptual model for our observations is presented in Figure 10. Initially (Figure 10a) the sample consists of polymer chains dotted with dye molecules. Increasing the pressure reduces the distances between

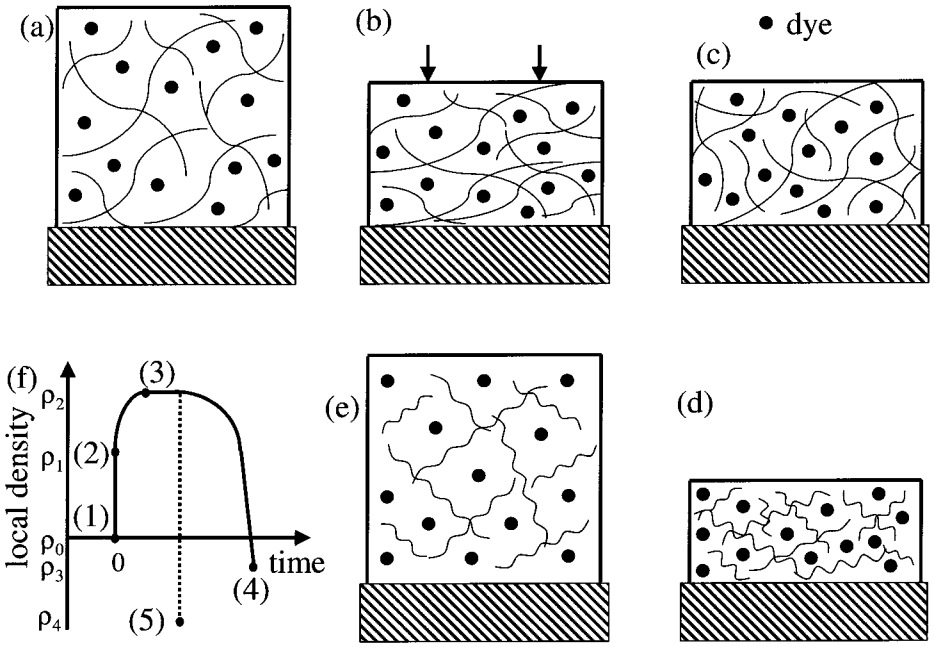

Figure 10. Conceptual model for nanoshock compression of a dye-doped polymer on a glass substrate. Open circles represent polymer chains, smaller solid circles represent dye molecules. (a) Initial configuration at density ρ_0. (b) After instantaneous response to a fast uniaxial compression, which increases the local density to ρ_1. In the second stage, the material loses strength and compresses further to density ρ_2. The second stage involves a combination of shear and volume relaxation. (c) Pure shear relaxation occurs by rearranging the polymer chains, producing a state of uniform stress, approaching hydrostatic stress. (d) Pure volume relaxation occurs as the chains adopt conformations which increase their density, as depicted by crinkling the polymer chains. (e) After unloading, some of the sample volume recovers, but the polymer chains remain trapped in a partially densified state. The dye sees a local density ρ_3 which is lower than the original density ρ_0. (f) Time dependence of the local density initially ("1"), after instantaneous compression ("2"), after the second stage of slower compression ("3"), and after unloading ("4"). The point "5" represents the hypothetical situation where unloading was complete and instantaneous.

polymer chains and between the chains and the dye. The dye is essentially incompressible. The polymer chains themselves are somewhat compressible because folded organic polymers or biopolymers typically have densities 10−20% lower than crystals of the monomer.[7] The time dependence of the ensemble average *local density* is depicted in Figure 10f. Before the shock (point "1" in Figure 10f) the volume is V_0, the bulk density is ρ_0, and the local density is ρ_0.

The sample is uniaxially compressed by a steeply rising shock front (Figure 10b), which corresponds to a vertical transition to the shocked region of the landscape. The volume decreases by an amount $\Delta V_1/V_0$, and the local density increases to ρ_1 (point "2" in Figure 10f). In our PMMA experiments, $\rho_1 \approx 1.14\ \rho_0$. Due to inertial confinement, the stress is a combination of uniaxial (*z*-axis) stress and shear stress. In the viscoelastic regime, the shear stress exceeds the material strength, so the material softens and becomes more compressible.

In the second viscous relaxation stage (Figure 10c,d) there is a combination of shear relaxation and volume relaxation. To illustrate, pure shear relaxation is depicted in Figure 10c and pure volume relaxation is depicted in Figure 10d. Pure shear relaxation involves a shape change without a volume change.[35] For shear relaxation, barriers on the shocked energy landscape must be overcome. The shear relaxation process tends to result in a stress tensor which is closer to diagonal and a state which is closer to the hydrostat. In uniaxial compression with lateral confinement, that can occur only by rearranging the polymer chains. The net motion of chains during shear relaxation is along a diagonal ±45 degrees from the compression axis.[35] Polymer chains that were adjacent before shear relaxation may no longer be adjacent—other chains may have been shoved into the regions between them. The original ordered structure of polymer chains is destroyed during extensive shear relaxation.

The pure volume relaxation process illustrated in Figure 10d occurs because the polymer chains go over barriers that permit them to adopt conformations that increase the density of each folded polymer chain and that allow the folded chains to pack tighter. This volume relaxation process is depicted schematically in Figure 10d by crinkling the polymer chains. The existence of energetic barriers to volume relaxation is proven by prior observations of densification of polymers by solidifying them at high pressure.[11]

The second stage of volume relaxation increases the local density seen by the dye probe, partly accounting for the second stage of the dye vibrational blue shift. In the second stage of compression, the density increases from ρ_1 to ρ_2 (to the point "3" in Figure 10f), where $\rho_2 \approx 1.3\ \rho_0$. However, it should be noted that pure shear relaxation could also account for part of the blue shift. Although shear relaxation does not change the *bulk density*,[35] it might affect the *local density* seen by the dye probe, by causing the polymer chains to pack more efficiently around the contours of the dye molecules.

The unloading process is depicted in Figure 10e. The sample expands and simultaneously the polymer chains themselves swell, but the average fractional increase in the volume of each polymer chain is not as large as the fractional increase in the bulk sample volume, creating the state where the dye registers negative pressure, as mentioned above. This requires further discussion.

Consider the following limiting case. The sample expands back to its original volume and density, but the polymer chains do not expand back fully to their original density. Instead only the elastic part comes back. Assuming the elastic part is not much affected by the structural relaxation, the elastic expansion would have the same magnitude as the elastic compression. In expanding back to its original volume, the sample fractional

volume increase is $(\Delta V_1 + \Delta V_2)/V_0$. The fractional elastic volume increase of polymer chains is $\Delta V_1/V_0$. Now there is extra empty space between the chains (Figure 10e), so the dye molecules see a local density less than the original density. The local density decreases from ρ_2 to ρ_4 (the point "4" in Figure 10f), where $\rho_4 = (1 - \Delta V_2/V_0)\rho_0 \approx 0.89\rho_0$. The local density ρ_4 would then be about 11% less than ρ_0. As discussed above, an 11% density decrease is taken to correspond to a dye blue shift of about -5 cm^{-1} and a pressure of about -2.3 GPa.

Because the dye is an embedded strain gauge sensitive to the local density, the dye may display strains opposite in sign to an external strain gauge that measures the displacement of the sample surface.[43] The meaning of negative pressure in this case is that the sample is unstable to spontaneous expansion of the polymer chains back to their original volume, although barriers to volume expansion on the ambient landscape may make this expansion slow or improbable.

The observed dye red shift after expansion is -2 cm^{-1}, corresponding to about -1 GPa pressure and a local density decrease of about 5%, so the experimental value for the local density ρ_3 (point "5" in Figure 10f) is $\rho_3 \approx 0.95\ \rho_0$. Since the local density ρ_3 depends on the difference between the bulk density and the density of the polymer chains, there is a range of final states which result in the same dye red shift. The extremes of this range represent the possible range of final sample volumes. For example, if the polymer chains do not swell at all during unloading, the minimum possible sample volume consistent with our results is about 95% of the original volume. The maximum possible sample volume might even be greater than the original volume, although more likely it is about equal to the initial volume, in which case the sample returns to its original volume and the polymer chains swell from 77% of their original volume to about 92% of their original volume. We cannot say where within this range the final state lies, although that might be determined by using time-resolved laser interferometry[60,61] to directly measure the displacement of the sample surface.

D. Energy Landscape View. The energy landscape view can be used to understand how a nanoshock pulse produces the unique final state characterized by a negative dye blue shift (negative local density change or negative pressure). The maximum effect is produced by a pulse which, as shown by Figure 2d, (1) generates almost instantaneous compression causing a nearly vertical transition to the shocked landscape, (2) has a load duration τ_{load} long enough for complete relaxation on the shocked landscape, and (3) unloads almost instantaneously causing a nearly vertical transition back to the ambient landscape.[6]

The strain rate produced by nanoshock compression is huge. The theoretical maximum possible strain rate at 4.5 GPa is what one expects for a low viscosity liquid. Shock front rise times in water[62,63] have been estimated to be 1 ps, so the theoretical maximum strain rate is estimated at 2×10^{11} s^{-1}, that is a strain $\Delta L/L = 0.2$ with a rise time of 1 ps. The actual strain rate $d(\Delta L/L)/dt > 8 \times 10^9$ s^{-1}, since the nanoshock front rise time is known at present only to be less than 25 ps.

We do not know the extent of structural relaxation on the shocked landscape, because the load duration τ_{load} is not long enough to be certain that the relaxation runs to completion. Nevertheless, it is clear that extensive structural relaxation does take place, because the observed value of the parameter $f \approx 0.5$, which characterizes the relative amplitudes of the elastic and viscous processes, is rather large. Our value $f = 0.5$ is about the same as the largest value of f seen in published VISAR data on PMMA,[5] where τ_{load} is much longer. Also, in some viscoelastic models it is possible to calculate the theoretical maximum value of f. For example, in Mark Berg's model for viscoelastic nonpolar solvation,[25] knowing that Poisson's ratio cannot exceed[35] 0.5, one can show that f cannot exceed about 0.6.

The rate constant for structural relaxation on a landscape can be expressed in an Arrhenius form,[7]

$$k_{str} = A(\eta)\exp(-\Delta E/RT) \tag{14}$$

where $A(\eta)$ is a preexponential factor which increases with decreasing viscosity η, and ΔE is the barrier height. Our determination of the shock viscosity $\eta_{sh} \approx 3$ Pa·s suggests that structural relaxation is occurring in a fluid-like medium with the viscosity of glycerol. The ~300 ps viscous relaxation is about what one expects from time-resolved measurements of molecular rotation or solvation in fluids of similar viscosities.[25] How should we understand the shock viscosity?

It is clear that the shock viscosity must be radically different from the ordinary viscosity η. Initially the polymer samples are supercooled liquids far below their glass-transition temperatures T_g ($T_g = 105$ °C for PMMA).[7] Although there is a shock-induced temperature rise to ~150 °C, that alone is not enough to melt PMMA because T_g increases with increasing pressure. For infinitesimal changes in pressure, T_g in PMMA increases at the rate $dT_g/dP = 0.23$ K/MPa.[11] Free-volume models predict that T_g increases forever with increasing pressure,[64] so one might conclude that T_g is 1,000 K at 4.5 GPa. However, configurational entropy models predict a leveling off of T_g at high pressure.[64] We are not aware of any relevant data for PMMA, but experiments on polystyrene show that T_g does indeed level off, at $T_g \approx 300$ °C, near a pressure of ~0.3 GPa.[64,65] Thus, it is reasonable to conclude that T_g for PMMA at 4.5 GPa is 300 °C or greater. Therefore, the 4.5 GPa nanoshock could not possibly heat PMMA above T_g.

Rapid structural relaxation on the shocked landscape should be viewed as a consequence of enormous shear stresses, which far exceed the attractive forces between polymer chains. The shocked but still supercooled liquid is subjected to such great stress that it undergoes extensive and catastrophic plastic deformation, which permits the polymer chains to find structures closer to the minimum energy region of the landscape despite the substantial energy barriers between adjacent local minima. In this view, although the shock temperature rise from 25 to 150 °C helps drive the relaxation over the barriers, the principal cause of structural relaxation is the dramatic drop of viscosity by orders of magnitude from $\eta > 10^{12}$ Pa·s to $\eta_{sh} \sim 3$ Pa·s.

This view helps explain why all of the samples behave similarly under nanoshock compression. The polymer samples have a wide range of molecular weights, from 1.5×10^4 to 4×10^6 Daltons. PEO polymer has only a polymer backbone with no side groups, whereas the other polymers have side groups ranging in size from the OH group of PVA to the larger amino acid residues in BSA. These structural features are paramount in determining the polymer's material response to small-amplitude perturbations, but they become largely irrelevant when the shear stress is far greater than the material strength, consistent with the principle that as the shock pressure increases, small differences in molecular structure and intermolecular interactions do not matter much.[33]

The ~4 ns unloading process is very interesting. Not much is known about the behavior of viscoelastic materials with very fast unloading.[4,5] As mentioned above, if unloading were instantaneous, the final state would have a dye red shift of 5

cm^{-1}, corresponding to $P = -2.3$ GPa, whereas the observed values are about 2 cm^{-1} and -1 GPa. Thus, during the ~4 ns expansion process, some structural relaxation must occur, as depicted by the tilted arrow in Figure 2d. In fact the data show there is about 3 cm^{-1} worth of structural relaxation in ~4 ns. In the compression process, there is about 5 cm^{-1} worth of structural relaxation in ~300 ps. Therefore, structural relaxation during unloading occurs, on average, about twenty times slower than during compression, even though the strain rate during unloading is about 10^2 times slower than the strain rate during compression.

E. Unique Mechanical States. The state of the polymers and proteins after nanoshock compression and release is very interesting. There is a lot of strain energy stored in the polymer after the nanoshock. The strain energy is $-P\Delta V$. For a residual pressure of 1 GPa, corresponding to ~5% compression, the stored strain energy is ~50 MJ/m^3. Figure 10d suggests that the post-shock samples are more porous and might have greater permeability than the original material. There are a number of medical experiments involving shock-induced drug delivery through skin[39,40] and shock-induced cell killing,[41] which indicate that short-duration shock waves increase the permeability of biological membranes and tissues, and that the magnitude of this permeability increase is greater with larger strain rates,[66,67] consistent with our results so far.

6. Conclusion

With the high time resolution of the nanoshock technique and the sensitivity and selectivity of molecular spectroscopy, we can see the two-part viscoelastic response of polymers and proteins even in the higher pressure range where structural relaxation is too fast to monitor by conventional methods of shock compression science. The rate of structural relaxation induced by the steeply rising shock front is used to infer a quite small value for the shock viscosity for solid polymers and proteins, just a few Pa·s. This viscosity is understood as a consequence of ultrahigh speed shock loading and ultrafast plastic deformation. After an ultrafast cycle of shock compression and unloading, an embedded dye strain gauge shows an interesting state of negative pressure, meaning that the local density is temporarily less than the initial density. This unique state is understood by looking at the nature of transitions between regions of the energy landscape seen by the ambient polymers and the shocked polymers. These experiments on model systems provide new insights into problems of shock compression of biological tissues and membranes.

Acknowledgment. We are grateful to Dr. Robert Frey of the U.S. Army Research Laboratory for his helpful comments. This paper is based upon work supported by the National Science Foundation under award number DMR 9714843 and by the Medical Free-electron Laser Program, via the Office of Naval Research award N00014-95-0259. Additional acknowledgment is given to Air Force Office of Scientific Research contract F49620-97-1-0056. Thickness measurements were carried out in the Center for Microanalysis of Materials, University of Illinois, which is supported by the U.S. Department of Energy under grant DEFG02-91-ER45439.

References and Notes

(1) Tas, G.; Hambir, S. A.; Franken, J.; Hare, D. E.; Dlott, D. D. *J. Appl. Phys.* **1997**, *82*, 1080.

(2) Dlott, D. D.; Hambir, S.; Franken, J. *J. Phys. Chem. B* **1998**, *102*, 2121.

(3) Schuler, K. W. *J. Mech. Phys. Solids* **1970**, *18*, 277.

(4) Schuler, K. W.; Nunziato, J. W.; Walsh, E. K. *Int. J. Solids Struct.* **1973**, *9*, 1237.

(5) Schuler, K. W.; Nunziato, J. W. *Rheol. Acta* **1974**, *13*, 265.

(6) Kim, H.; Hambir, S. A.; Dlott, D. D. *Phys. Rev. Lett.* **1999**, *83*, 5034.

(7) Mark, H. F.; Bikales, N.; Overberger, C. G.; Menges, G.; Kroschwitz, J. I. *Encyclopedia of Polymer Science and Engineering*, Second Edition; Rapra Technology, Ltd.: Shawbury, Shrewsbury, Shropshire, United Kingdom, 1985−1990.

(8) Marvin, R. S.; McKinney, J. E. Volume relaxations in amorphous polymers. In *Physical Acoustics*; Mason, W. P., Ed.; Academic Press: New York, 1965; Vol. IIB.

(9) Stillinger, F. H. *Science* **1995**, *267*, 1935.

(10) Tammann, G.; Jenckel, E. *Z. Anorg-Allg. Chem.* **1929**, *184*, 416.

(11) Price, C. *Polymer* **1975**, *16*, 585.

(12) Mark, H. F.; Bikales, N.; Overberger, C. G.; Menges, G.; Kroschwitz, J. I. *Encyclopedia of Polymer Science and Engineering*, Second Edition; Rapra Technology, Ltd.: Shawbury, Shrewsbury, Shropshire, United Kingdom, 1985−1990; Vol. 17, pp 632−665.

(13) Barker, L. M.; Hollenbach, R. E. *J. Appl. Phys.* **1970**, *41*, 4208.

(14) Gupta, Y. M. *J. Appl. Phys.* **1980**, *51*, 5352.

(15) Johnson, J. N.; Dick, J. J.; Hixson, R. S. *J. Appl. Phys.* **1998**, *84*, 2520.

(16) Gustov, V. W. Polymerization and modification of polymers under shock compression. In *High-pressure Chemistry and Physics of Polymers*; Kovarskii, A. L., Ed.; CRC Press: Boca Raton, 1994; p 301.

(17) Hambir, S. A.; Kim, H.; Dlott, D. D. Ultrafast dynamics of nanoshocks in molecular materials. In *Shock Compression of Condensed Matter*−1999; Furnish, M. D., Ed.; American Institute of Physics: New York, 1999; in press.

(18) Barker, L. M.; Hollenbach, R. E. *J. Appl. Phys.* **1972**, *43*, 4669.

(19) Litovitz, T. A.; Davis, C. M. Structural and shear relaxation in liquids. In *Physical Acoustics. Principles and Methods*; Mason, W. P., Ed.; Academic Press: New York, 1965; p 282.

(20) Prieto, F. E.; Renero, C. *J. Appl. Phys.* **1973**, *44*, 4013.

(21) Swegle, J. W.; Grady, D. E. *J. Appl. Phys.* **1985**, *58*, 692.

(22) Rosenthal, S. J.; Xie, X.; Du, M.; Fleming, G. R. *J. Chem. Phys.* **1991**, *95*, 4715.

(23) Cho, M.; Rosenthal, S. J.; Scherer, N.; Ziegler, L.; Fleming, G. R. *J. Chem. Phys.* **1992**, *96*, 5033.

(24) Walsh, A. M.; Loring, R. F. *Chem. Phys. Lett.* **1991**, *186*, 77.

(25) Berg, M. *Chem. Phys. Lett.* **1994**, *228*, 317.

(26) Berg, M. *J. Phys. Chem. A* **1998**, *102*, 17.

(27) Tas, G.; Franken, J.; Hambir, S. A.; Dlott, D. D. *Phys. Rev. Lett.* **1997**, *78*, 4585.

(28) Dlott, D. D. *Annu. Rev. Phys. Chem.* **1999**, *50*, 251.

(29) Eesley, G. L. *Coherent Raman Spectroscopy*; Pergamon: Oxford, 1991.

(30) Hambir, S. A.; Franken, J.; Hare, D. E.; Chronister, E. L.; Baer, B. J.; Dlott, D. D. *J. Appl. Phys.* **1997**, *81*, 2157.

(31) Marsh, S. P. *LASL Shock Hugoniot Data*; University of California, Berkeley: Berkeley, CA, 1980.

(32) Lee, I.-Y. S.; Hill, J. R.; Dlott, D. D. *J. Appl. Phys.* **1994**, *75*, 4975.

(33) Graham, R. A. *Solids Under High-Pressure Shock Compression. Mechanics, Physics and Chemistry*; Springer-Verlag: New York, 1993.

(34) Franken, J.; Hambir, S.; Hare, D. E.; Dlott, D. D. *Shock Waves* **1997**, *7*, 135.

(35) Zel'dovich, Y. B.; Raiser, Y. P. *Physics of Shock Waves and High-temperature Hydrodynamic Phenomena*; Academic Press: New York, 1966.

(36) Stillinger, F. H.; Weber, T. A. *Phys. Rev. A* **1983**, *28*, 2408.

(37) Stillinger, F. H. *J. Phys. Chem. B* **1998**, *102*, 2807.

(38) Stillinger, F. H. *Phys. Rev. E* **1999**, *59*, 48.

(39) Lee, S.; McAuliffe, D. J.; Flotte, T. J.; Kollias, N.; Doukas, A. G. *J. Invest. Dermat.* **1998**, *111*, 925.

(40) Lee, S.; Kolias, N.; McAuliffe, D. J.; Flotte, T. J.; Doukas, A. G. *Pharm. Res.* **1999**, *16*, 1717.

(41) Lin, C. P.; Kelly, M. W.; Sibayan, S. A. B.; Latina, M. A.; Anderson, R. R. *IEEE J. Sel. Top. Quantum Electron.* **1999**, *5*, 1.

(42) Bloomquist, D. D.; Sheffield, S. A. *Bull. Am. Phys. Soc.* **1979**, *24*, 714.

(43) Cagnoux, J.; Chartagnac, P.; Hereil, P.; Perez, M. *Ann. Phys. Fr.* **1987**, *12*, 451.

(44) Lee, I.-Y. S.; Tolbert, W. A.; Dlott, D. D.; Doxtader, M. M.; Foley, D. M.; Arnold, D. R.; Ellis, E. R. *J. Imag. Sci. Technol.* **1992**, *36*, 180.

(45) Lee, I.-Y. S.; Hill, J. R.; Suzuki, H.; Baer, B. J.; Chronister, E. L.; Dlott, D. D. *J. Chem. Phys.* **1995**, *103*, 8313.

(46) Berg, M. A.; Hubble, H. W. *Chem. Phys.* **1998**, *233*, 257.

(47) Johnson, J. N.; Barker, L. M. *J. Appl. Phys.* **1969**, *40*, 4321.

(48) Frauenfelder, H.; Alberding, N. A.; Ansari, A.; Braunstein, D.; Cowen, B. R.; Hong, M. K.; Iben, I. E. T.; Johnson, J. b.; Luck, S.; Mardes, M. C.; Mourant, J. R.; Ormos, P.; Reinisch, L.; Scholl, R.; Schulte, A.; Shyamsunder, E.; Sorensen, L. B.; Steinbach, P. J.; Xie, A.; Young, R. D.; Yue, K. T. *J. Phys. Chem.* **1990**, *94*, 1024.

(49) Califano, S.; Schettino, V.; Neto, N. *Lattice Dynamics of Molecular Crystals*; Springer-Verlag: Berlin, 1981.
(50) Ashcroft, N. W.; Mermin, N. D. *Solid-state physics*; Holt, Reinhart and Winston: New York, 1976.
(51) Lacks, D. J. *Phys. Rev. Lett.* **1998**, *80*, 5383.
(52) Malandro, D. L.; Lacks, D. J. *J. Chem. Phys.* **1997**, *107*, 5804.
(53) *High-Pressure Chemistry*; Kelm, H., Ed.; D. Reidel Co.: Dordrecht, Holland, 1978.
(54) Beaumont, P. C.; Johnson, D. G.; Parsons, B. J. *J. Chem. Soc., Faraday Trans.* **1998**, *94*, 195.
(55) Narasimhan, L. R.; Littau, K. A.; Pack, D. W.; Bai, Y. S.; Elschner, A.; Fayer, M. D. *Chemical Rev.* **1990**, *90*, 439.
(56) Maroncelli, M.; MacInnis, J.; Fleming, G. R. *Science* **1989**, *243*, 1674.
(57) Stratt, R. M.; Maroncelli, M. *J. Phys. Chem.* **1996**, *100*, 12981.
(58) Barbara, P. F.; Jarzeba, W. Ultrafast photochemical intramolecular charge transfer and excited-state solvation. In *Advances in Photochemistry*; Volman, D. H., Hammond, G. S., Gollnick, K., Eds.; John Wiley and Sons: New York, 1990; Vol. 15; p 1.
(59) Franken, J.; Hambir, S. A.; Dlott, D. D. *J. Appl. Phys.* **1999**, *85*, 2068.
(60) Albagli, D.; Dark, M.; Perelman, L. T.; von Rosenberg, C.; Itzkan, I.; Feld, M. S. *Opt. Lett.* **1994**, *19*, 1684.
(61) Furutani, H.; Fukumura, H.; Masuhara, H. *Appl. Phys. Lett.* **1994**, *65*, 3413.
(62) Harris, P.; Presles, H.-N. *J. Chem. Phys.* **1982**, *77*, 5157.
(63) Leung, K. P.; Doukas, A. G.; Jones, P. H.; Papadimitriou, D.; Alfano, R. R.; Harris, P. *Phys. Rev. B* **1985**, *31*, 8329.
(64) Mark, H. F.; Bikales, N.; Overberger, C. G.; Menges, G.; Kroschwitz, J. I. *Encyclopedia of Polymer Science and Engineering*, Second Edition; Rapra Technology, Ltd.: Shawbury, Shrewsbury, Shropshire, United Kingdom, 1985−1990; Vol. 17, pp 1−47.
(65) Stevens, J. R.; Croakley, R. W.; Chau, K. W.; Hunt, J. L. *Annal. NY Acad. Sci.* **1986**, *484*, 324.
(66) McAuliffe, D. J.; Lee, S.; Flotte, T. J.; Doukas, A. G. *Lasers Surg. Med.* **1997**, *20*, 216.
(67) Mulholland, S. E.; Lee, S.; McAuliffe, D. J.; Doukas, A. G. *Pharm. Res.* **1999**, *16*, 514.